Analysis of Finite-Sized Tapered Slot Antennas

Arzu Keskin[1], Adnan Köksal[2]

[1] Department of Electrical and Electronics Engineering
Hacettepe University
arzukkeskin@gmail.com
[2] Departmentof Electrical and Electronics Engineering
Hacettepe University
koksal@hacettepe.edu.tr

Abstract

An analysis of the Linearly Tapered Slot Antenna (LTSA) on a finite dielectric substrate has been developed by using A Method of Moments (MoM). An approximate closed form Green's function is obtained for the infinite dielectric substrate. Galerkin type Method of Moments with RWG basis functions are used in order to solve Electric Field Integral Equation (EFIE) derived for the LTSA. Finite dielectric substrate region is modelled by equivalent volume polarization currents existing in this region. The feed section of the antenna is modelled with a pulse excitation. Modifying the incident field using the polarization current density, and solving for the antenna currents in air yields accurate results without increasing the number of unknowns as in the full-wave model. Comparisons of small and large LTSA patterns with HFFS results are presented to demonstrate the validity of the model.

1. Introduction

The Linearly Tapered Slot Antenna is a member of travelling wave antennas and operates over a large bandwidth. LTSA was first introduced by Gibson [1], and has become an important element for the millimetre wave and microwave applications [2]. Janaswamy presented the first analytical solution for the LTSA [4]. In the analysis, he approximated the antenna taper step-wise and solved each section as an eigenvalue problem for a slot line, to determine the aperture field up to a multiplicative constant in each slot line section [5]. Enforcing the power conservation principle then enables to determine the aperture distribution, and the pattern of the antenna is obtained by using equivalent magnetic currents in the presence of a perfectly conducting half plane. Unfortunately, this method assumes conductors with infinite width and length, and it is particularly accurate for long antennas ($L >> 3\lambda$). Later, Köksal and Kauffman considered the actual geometry of the antenna and analysed LTSAs on a finite dielectric substrate by using MoM [6]. In this work, LTSAs on a finite dielectric substrate is analysed by a two-step MoM. Initially, approximate spectral-domain Green's functions for an infinite dielectric substrate are obtained by using the discrete complex image method, and the spatial-domain Green's functions are obtained as a closed form approximation. In the first step of the analysis, the Green's functions expressed in closed forms using the complex images are used in the MoM solution of the electric field integral equation, and the current density on the conducting parts of the antenna is obtained. In the second step, the effect of the finite dielectric region is modelled with volume polarization currents, and the incident field vector is modified using the fields of these polarization currents. The solution of the EFIE for the antenna in air, for currents on the conducting parts of the antenna with this new voltage vector yields the solution for the currents. Far field patterns of the antennas in the E and H planes are compared with HFFS simulation results and with the far field pattern expressions reported earlier [5].

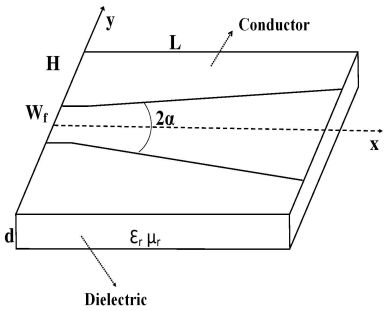

Figure 1. LTSA Geometry

2. The Method

The geometry of the LTSA is shown in Fig 1. The aim of this work is to characterize the radiated far-fields of a single LTSA on a finite-sized dielectric substrate as antenna parameters length (L), height (H), taper angle (α), substrate thickness (d), and the relative permittivity (ϵ_r) vary. The ranges of these parameters are chosen as:

$$0.25\lambda_0 \leq L \leq 5\lambda_0$$
$$0.25\lambda_0 \leq H \leq 3\lambda_0$$
$$2.5^0 \leq \alpha \leq 9^0$$
$$0.01\lambda_0 \leq d \leq 0.1\lambda_0$$
$$1 \leq \epsilon_r \leq 10.5$$

The EFIE derived for the LTSA can be given as

$$\vec{E}^i_{tan}(\vec{r}) = j\omega \int_S \vec{G}^A(\vec{r},\vec{r}')\ \vec{J}_s(\vec{r}')\ ds' -$$

$$\frac{1}{j\,\omega} \int_S \nabla \left(\nabla \cdot \vec{J}_s(\vec{r}') \right)\ G^q(\vec{r},\vec{r}')\ ds' \tag{1}$$

where $\vec{J}_s(\vec{r}')$ is the induced current density, $\vec{E}^i_{tan}$ is the tangential incident electric field, $\vec{G}^A$ is the vector potential Green's function, G^q is the scalar potential Green's function, $\vec{r}$ is the observation point, and $\vec{r}'$ is the source point. In order to solve the EFIE, vector and potential Green?s function of the layered media are obtained using 3-level Discrete Complex Image Method (DCIM) initially. The spatial-domain Green's functions are obtained by using the Hankel transformation of the corresponding spectral-domain Green's functions as

$$G(\rho) = \frac{1}{4\pi} \int_{SIY} dk_\rho\ k_\rho\ H_0^{(2)}(k_\rho \rho)\ \tilde{G}\,(k_\rho) \tag{2}$$

where SIP stands for the Sommerfeld integration path, $H_0^{(2)}$ is the zeroth order Hankel function of second kind, and $\tilde{G}\,(k_\rho)$ is the spectral-domain Green's function in k_ρ domain [9]. Since kernel of the Sommerfeld integral is oscillatory, and its computation is time consuming, this integral is approximated using closed-forms Green's function (CFGF). Spatial domain Green's function is obtained by using 3-level DCIM. In doing so, the spectral-domain Green's functions are sampled along three-paths on complex k_ρ plane [10].

Once the closed-form approximations of spatial domain Green's functions are obtained, they are used in the EFIE given in Eqn. (1). Using MoM, the EFIE is discretized by using RWG basis functions and Galerkin type testing. Doing so results in

$$\int_{S_m} \vec{E}^i_{tan}\ \cdot\ \vec{f}_m(\vec{r})\ ds =$$

$$\int_{S_m} \vec{f}_m(\vec{r}) \cdot \left[\sum_{n=1}^{N} j\omega \left[\int_{S_n} B_n\ \vec{f}_n(\vec{r}') \right] \right] \vec{G}^A(\vec{r},\vec{r}')ds' +$$

$$\int_{S_m} \vec{f}_m(\vec{r}) \cdot \left[\sum_{n=1}^{N} j \left[\frac{1}{\omega} \int_{S_n} \nabla\nabla \cdot B_n\ \vec{f}_n(\vec{r}') \right] \right]\ G^q(\vec{r},\vec{r}')ds' \tag{3}$$

and by rearranging Eqn. (3), the moment method matrix equation is obtained as:

$$[Z_{mn}]\,[\alpha] = V_m \tag{4}$$

The solution of this matrix equation gives the unknown conductor currents.

In this solution procedure, the feed section of the antenna is modelled with a pulse source.

The far-field pattern of the antenna can be found using the calculated antenna currents as:

$$\vec{F}\,(\theta,\phi) = \int_{S'} \sum_{n=1}^{N} a_n \vec{f}_n(\vec{r}')e^{j\vec{k}\vec{r}'}\,dr' \tag{5}$$

$$\vec{k} = k\,(\hat{a}_x \sin\theta\cos\phi + \hat{a}_y \sin\theta\sin\phi + \hat{a}_z \cos\theta) \tag{6}$$

After obtaining the surface current density, the dielectric substrate geometry is divided into cubical sections. The electric field in the middle of each segment can be written in terms of the surface current density and the associated closed-form Green's function, derived for the vector and scalar potentials as follows:

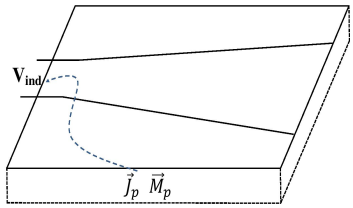

Figure 2. The effect of polarization currents as the source

$$\vec{E}(\vec{r}) = -j\,\omega \int_S \vec{G}^A(\vec{r},\vec{r}')\ \vec{J}_s(\vec{r}')\ ds' +$$

$$\nabla \left[\nabla \cdot \frac{1}{j\,\omega} \int_S \vec{J}_s(\vec{r}')\ G^q(\vec{r},\vec{r}')\ ds' \right] \tag{7}$$

The equivalent polarization currents can be written as:

$$\vec{J_p} = j\omega(\epsilon - \epsilon_0)\vec{E} \tag{8}$$

The far field pattern of the polarization currents in return is given as

$$\vec{F}(\theta,\phi) = \int \vec{J_p}(\vec{r'})e^{\vec{k}\vec{r}'}\,d\vec{r}' \tag{9}$$

After completing the modelling for the conductor and dielectric regions, the effect of the polarization currents on the voltage vector is calculated.

In order to model this effect, the right hand side of (2) is modified by the amount as given below:

$$V_m = \int_{Sc} \vec{E} \left\{ \vec{J_p} \right\} \cdot \vec{J_c}\ ds \tag{10}$$

The EFIE given in Eqn. (3) is solved again without any substrate to obtain the final surface current density on the LTSA. By using the procedure outlined, the radiation characteristic of the LTSA has been analysed. The results obtained with the explained procedure are compared to those obtained earlier by Janaswamy [5]. The patterns in Janaswamy's work are obtained using the far field due to an x-directed two sided infinitesimal slot located at (x', z') on a conducting half-plane given as

$$\hat{e}_{\theta,\,janas}(\theta,\phi) = |\sin\phi|\,e^{\,j\pi/4}\ F(v)\,e^{\,jk_0(x'\sin\theta\cos\phi + z'\cos\theta)}$$

$$+ \frac{\frac{\sin\phi}{2} e^{-j[\pi/4 + k_0(x'\sin\theta - z'\cos\theta)]}}{\sqrt{\pi k_0 x'\sin\theta}} \tag{11}$$

where $v = k_0 x'\sin\theta\ (1+\cos\phi)$, and $F(v)$ is the Fresnel integral. After finding the aperture electric field, the radiation characteristics of the LTSA is obtained in [5] as follows:

$$E^i_{\theta,\,janas} = \hat{e}_{\theta,\,janas}(\theta,\phi).E^i_a \tag{12}$$

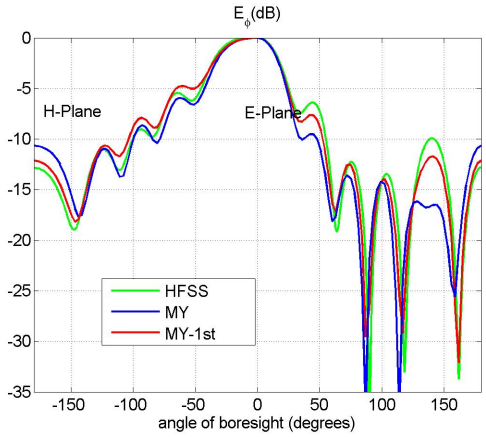

Figure 3. E-Plane pattern for an LTSA with $\epsilon_r = 2.2$ ($L = 2\lambda_o$, $H = 0.5\lambda_o$, $W_f = 0.06\lambda_o$, $d = 0.017\lambda_o$, $\alpha = 7^o$).

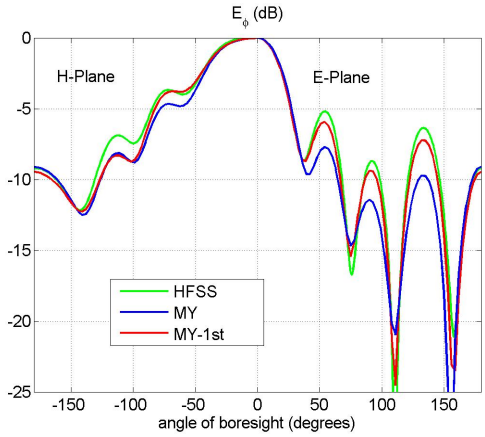

Figure 4. E-Plane pattern for an LTSA with $\epsilon_r = 2.2$ ($L = 1.5\lambda_o$, $H = 0.375\lambda_o$, $W_f = 0.06\lambda_o$, $d = 0.017\lambda_o$, $\alpha = 7^o$).

3. RESULTS AND DISCUSSION

The analysis presented in the previous section is cast into a MoM code and results for various dimensions and permittivity values are obtained. In this section, the accuracy of E and H plane patterns of these antennas are investigated by comparing our results to simulation program HFSS, and to results of earlier reported approximate method of Janaswamy. In the figures, the results obtained with HFSS, Janaswamy's far field expression and our analysis are compared. Equation (11) goes to infinity for $\theta = 90^o$, and hence the patterns obtained by Janaswamy's theory are calculated up to $\theta = 90^o$. Label MoM shows our initial MoM results, while MoM-1st shows the results of our two-step procedure using the effect of polarization.

With the coordinate system of Fig. 1, E-plane of the antenna coincides with the $x-y$ plane, while H-plane is the $x-z$ plane. To be able to obtain E-plane $\theta = 90$, $\phi \rightarrow [0, 180]$, while for H-plane $\phi = 0$, $\phi \rightarrow [90, 0]$ and $\phi = \pi$, $\theta \rightarrow [0, 90]$ planes are considered.

Fig. 3- Fig. 5 shows the radiation characteristics for a LTSA with different dimensions and the results using our method are consistent with HFSS simulation results.

Fig. 6 and Fig. 7 show the comparison for the E and H plane patterns for an LTSA with $L = \lambda_o$, $H = 0.5\lambda_o$, $W_f = 0.06\lambda_o$, $d = 0.017\lambda_o$, $\alpha = 7^o$, $\epsilon_r = 2.2$. Very good agreement is observed between our method and HFSS results, while big differences occur in the results obtained by the method of Janaswamy. Fig. 8 and Fig. 9 show the comparison for large antennas for which the dimensions are $(L = 4\lambda_o, H = \lambda_o)$, and $(L = 5\lambda_o, H = 1.5\lambda_o)$, respectively with $W_f = 0.06\lambda_o$, $d = 0.017\lambda_o$, $\alpha = 7^o$, and $\epsilon_r = 2.2$. As can be seen easily from Fig. 8 and Fig. 9, the accuracy is better than Janaswamy's method yields. Fig. 10 and Fig. 11 present the results of a parametric study of an LTSA with respect to dielectric constant. It can be seen from these figures that, as the permittivity increases, sidelobe level in the E-Plane increases, and the beamwidth in the H-Plane decreases. Similar studies and results have shown that the method presented in this work offers reliable and more accurate results, especially when the antenna size is small, as most of the time is preferred.

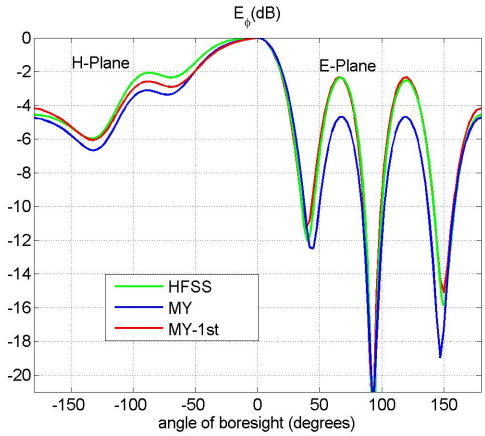

Figure 5. E-Plane pattern for an LTSA with $\epsilon_r = 2.2$ ($L = \lambda_o$, $H = 0.25\lambda_o$, $W_f = 0.06\lambda_o$, $d = 0.017\lambda_o$, $\alpha = 7^o$).

4. Conclusion

In this work, a two-step MoM procedure is presented for LTSAs on a finite dielectric substrate. The procedure consists of solving for the antenna currents by closed-form Green's function, assuming infinite dielectric substrate initially, then modifying the excitation vector using the polarization currents of the finite substrate, and solving for the conductor currents of the antenna in the air. The results obtained using the presented method display good agreement with HFSS results.

In the case of small size antennas, big errors occur in the results obtained using earlier reported methods, whereas the results of this work display good accuracy. It is believed that, modelling the polarization current in the finite dielectric substrate is the reason for this increased accuracy.

For large antennas, the method reported in this work still gives accurate results, however the computational cost must be considered as an issue in those cases, since the same problem is solved twice, first for the dielectric supported antenna, and the second for the air LTSA case, with modified excitation or voltage vector using the effect of the polarization in the finite dielectric.

It is worthwhile to mention that, the method reported in this paper can be applied directly to other antennas with finite-sized

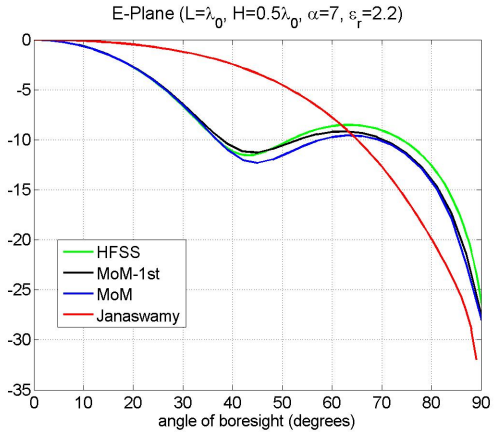

Figure 6. E-Plane pattern for an LTSA with $\epsilon_r = 2.2$ ($L = \lambda_o$, $H = 0.5\lambda_o$, $W_f = 0.012\lambda_o$, $d = 0.017\lambda_o$, $\alpha = 7^o$).

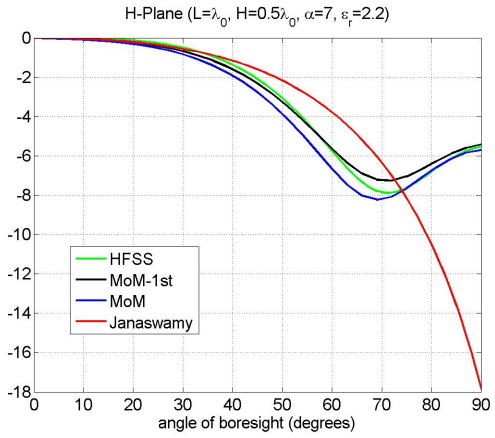

Figure 7. H-Plane pattern for an LTSA with $\epsilon_r = 2.2$ ($L = \lambda_o$, $H = 0.5\lambda_o$, $W_f = 0.012\lambda_o$, $d = 0.017\lambda_o$, $\alpha = 7^o$).

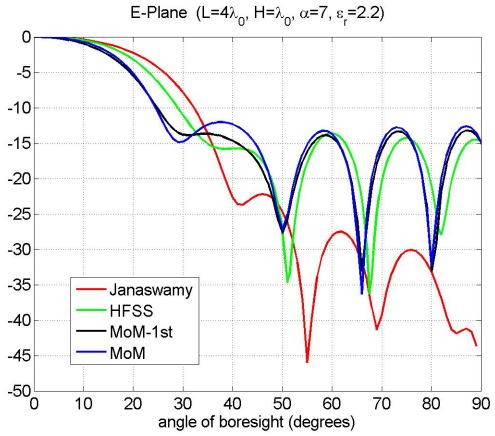

Figure 8. E-Plane pattern for an LTSA with $\epsilon_r = 2.2$ ($L = 4\lambda_o$, $H = \lambda_o$, $W_f = 0.012\lambda_o$, $d = 0.017\lambda_o$, $\alpha = 7^o$).

dielectric substrate, for example to microstrip patch antennas.

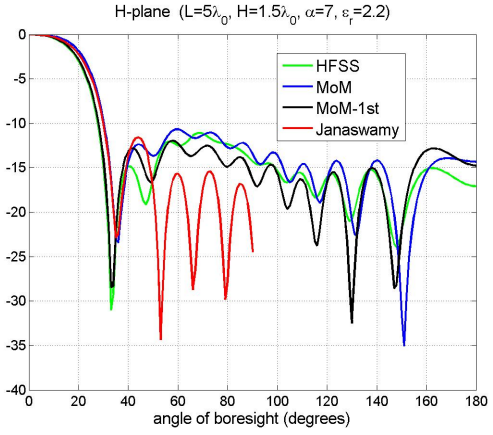

Figure 9. H-Plane pattern for an LTSA with $\epsilon_r = 2.2$ ($L = 5\lambda_o$, $H = 1.5\lambda_o$, $W_f = 0.012\lambda_o$, $d = 0.017\lambda_o$, $\alpha = 7^o$).

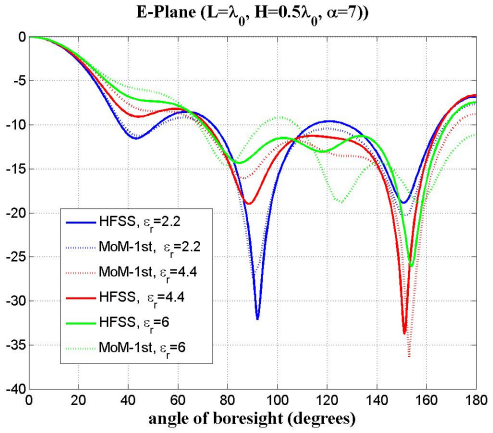

Figure 10. Variation of the E-Plane pattern for an LTSA with $\epsilon_r = 2.2$, $\epsilon_r = 4.4$, $\epsilon_r = 6$ ($L = \lambda_o$, $H = 0.5\lambda_o$, $W_f = 0.012\lambda_o$, $d = 0.017\lambda_o$,$\alpha = 7^o$)

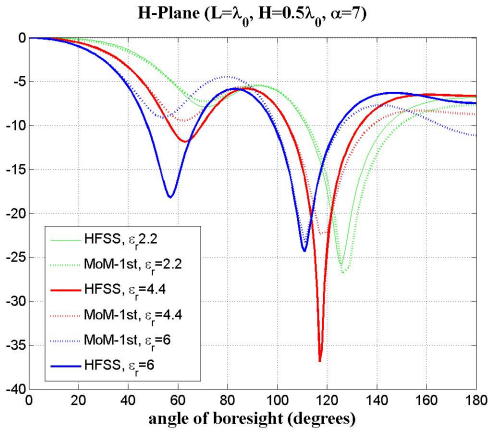

Figure 11. Variation of the H-Plane pattern for an LTSA with $\epsilon_r = 2.2$, $\epsilon_r = 4.4$, $\epsilon_r = 6$ ($L = \lambda_o$, $H = 0.5\lambda_o$, $W_f = 0.012\lambda_o$, $d = 0.017\lambda_o$,$\alpha = 7^o$)

5. References

[1] P. J. Gibson, "The Vivaldi Aerial", in *Proc. 9th European Microwave Conf.*, Brighton, U.K., 1979, pp. 101-105.

[2] G. M. Rebeiz, "Millimeter-Wave and Terahertz Integrated Circuit Antennas", *Proceedings of the IEEE*, vol. 80, no.11, pp: 1748-1770, 1992.

[3] R. Janaswamy, "Radiation Pattern Analysis of the Tapered Slot Antenna", Ph.D. thesis, Massachusetts. Univ., USA., 1986.

[4] R. Janaswamy, "An Accurate Moment Method Model for The Tapered Slot Antenna", *IEEE Trans. Antennas Propagat.*, vol. AP-37, no.x, pp: 1523-1528, December, 1989.

[5] R. Janaswamy R., D. H. Schaubert, "Analysis of the Tapered Slot Antenna", *IEEE Trans. Antennas Propagat.,*, vol. AP-35, , pp: 1058-1064, 1987.

[6] A. Köksal and J. F. Kauffman, "Moment Method Analysis of Linearly Tapered Slot Antennas", *Int Journal of Microwave and Millimeter-Wave CAE 4*, pp: 76-87, 1994.

[7] A. Köksal, "Moment Method Analysis of Linearly Tapered Slot Antennas", Ph.D. thesis, *Department of Electrical and Computer Eng.*, North Carolina State Univ., Raleigh, November, 1992.

[8] M. I. Aksun and G. Dural, "Clarification of Issues on the Closed-Form Greens Functions in Stratified Media", *IEEE Trans. on Antennas and Propagation*, vol. 53, no.11, pp: 3644-3653, November, 2005.

[9] M. I. Aksun and N. Kinayman, "Modern Microwave Circuits", *Artech House*, 2005.

[10] A. Alparslan, "Study of Green's Functions of Potentials and Fields in Layered Media Composed of Left-handed and Right-handed Materials", M.S. thesis, *Department of Electrical and Computer Eng.*, Koç Univ., İstanbul, Turkey, 2008.